Scientific Visualization, 2022, volume 14, number 4, pages 52 - 61, DOI: 10.26583/sv.14.4.05

The Discharge Heated Channel Region Visualization based on Thermal Imaging Registration

I.A. Znamenskaya[1], E.A. Karnozova[2], T.A. Kuli-Zade[3]

Lomonosov MSU (Moscow State University), Department of Physics

[1] ORCID: 0000-0001-6362-9496, znamen@phys.msu.ru
[2] ORCID: 0000-0001-9611-443X, karnozova.ea16@physics.msu.ru
[3] ORCID: 0000-0003-0249-6292, tahir@physics.msu.ru

Abstract

The paper presents the results of non-stationary thermal fields panoramic visualization, based on infrared thermography at the STDO-3 device (Shock Tube – Discharge – Optics) of the Lomonosov Moscow State University, Faculty of Physics. The main purpose of the work was to study the heating and cooling processes in a rectangular channel region under the influence of pulsed surface high-current discharges sliding over the dielectric surface, taking into account the supersonic flow in a channel with an obstacle. A pulsed surface discharge initiated in a 24x48 mm2 channel was studied in a quiescent air and in a high-speed flow behind the shock. When initiated in the flow (the delay time after the shock wave passage is up to 0.4 ms), the discharge plasma is localized mainly in the downwind region behind the reverse step (rectangular ledge). The discharge produces a pulsed (submicrosecond) contracted energy input with a 30 mm length in the localization zone. As a result, there is a short-term heating of the section of the channel wall adjacent to it. Using infrared (IR) thermographic imaging through the chamber quartz windows transparent to IR radiation, it was found that in the discharge chamber the discharge plasma noticeably heats the surface of the flat channel wall. Based on the obtained data of panoramic visualization with an exposure time up from 200 μs, we studied the channel walls cooling process both in quiescent air and in flow at different oncoming gas velocities – in the downwind region behind the dielectric ledge.

Keywords: infrared thermography, panoramic visualization, thermal fields evolution, high-speed shooting, nanosecond discharge, high speed flow, shock waves.

1. Introduction

The high-speed thermographic technology development leads to the possibility of visualization and registration of rapidly changing thermal fields generated by non-stationary gas flows, in particular, the gas-dynamic flow boundary layer region characteristic.

Rapid (on a nanosecond time scale) heating of gas is of the greatest interest in the problems of flow control using pulsed discharge plasma. The heat released during the nanosecond surface discharges plasma initiation is distributed mainly through two ways: the rapid air heating near the wall and the dielectric material layer heating [1 – 6]. Later, the convective heat exchange process occurs between the dielectric material layer and the heated air. To study the temperature fields during the nanosecond dielectric barrier discharge (NS-DBD) initiation [4], the results obtained based on IR thermography and optical emission spectroscopy were compared. An analysis of the results showed that the plasma rotational temperature obtained using optical emission spectroscopy turned out to be close to the temperature measured using IR thermography, which means that the gas temperature in the used discharge can be approximately represented by the rotational temperature.

Based on a combination of high-speed schlieren registration and infrared thermography studies were conducted on the influence of a number parameters (trigger voltage, repetition

rate, electrode size) on discharge characteristics, induced the NS-DBD discharge flow fields and thermal characteristics [5]. The electrode surface temperature distributions with a changing flow field for 120 s (the plasma actuator operating time – induced by NS-DBD) were recorded using thermal imaging. In this case, the thermal imager was located close to the surface area where the discharge was initiated; therefore, the radiated power attenuation caused by the absorption and scattering of various components in the air was neglected. The eternal copper electrode surface temperature was not analyzed due to its relatively lower surface emissivity [6, 7].

Despite a large number of works studying the influence of actuators on the flow, thermal fields in high-speed unsteady flows are considered extremely rarely [3, 8]. In most studies of infrared thermography, the method was mainly applied to study the discharge thermal effect in the high-frequency mode when it was initiated in a subsonic flow or in stationary gas flows in a wind tunnel.

2. Installation and panoramic registration.

A special discharge section (Fig. 1) with transparent quartz glass side walls (optical windows) 16 mm thick was built into the single-diaphragm shock tube low-pressure channel with a 24 × 48 mm² [9] rectangular cross size. Through the discharge section side walls, high-speed recording methods (shadowgraph method, optical glow registration, thermal imaging) were used to study the effect on the high-speed flow from a distributed surface discharge sliding over the dielectric surface in the space between copper plasma electrodes mounted flush on the dielectric surfaces of the upper and lower walls [10]. The surface discharge was simultaneously initiated on the upper and lower discharge section walls and represented two thin plasma layers (plasma sheets). The area of each plasma sheet was 100 × 30 mm². Both discharges had a multichannel structure: each discharge was a set of parallel plasma microchannels 30 mm long, distributed over the dielectric surface 100 mm long and spaced 9 mm (electrode width) from each of the side walls.

A dielectric caprolon ledge, 48 × 6 × 2 mm³ in size, was installed on the lower channel wall between two optical windows at a 20 mm distance from one edge of the lower plasma electrode. The ledge existence created a 6-mm gap in the lower plasma layer, which changed the local discharge electric field distribution, thereby increasing the local pulsed energy input – near the step, the value of the rapidly thermalized discharge energy increases by a factor of 5–7 compared to the average thermalized energy concentration values in the upper plasma sheet [10].

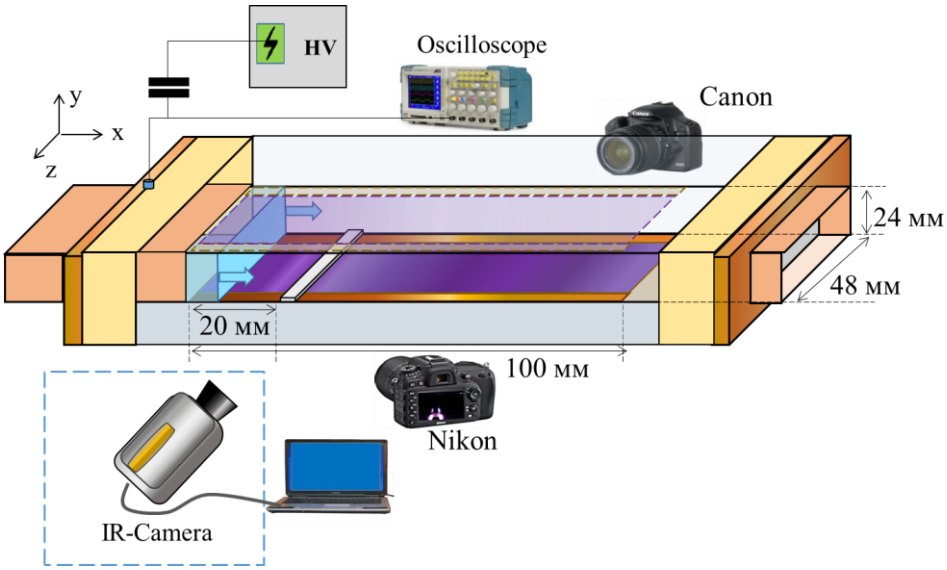

Figure 1. The operating section scheme.

The results obtained by high-speed registration methods were used to determine quantitative data of the bright channels maximum radiation time in the optical and infrared ranges on the pressure dependence.

Data on the evolution of the surface discharge plasma glow initiated in initially quiescent air were recorded in the optical (Bifo KO11 camera – nine-frame shooting, exposure 100 ns, time between frames 100 ns) range and thermal fields panoramic visualization was carried out (thermographic photography in the transmission range of the discharge section quartz windows) after the discharge. The optical glow photographs recorded by a high-speed 9-frame camera were compared with the integral discharge glow images. Integral discharge plasma glow shooting obtained from two angles with digital cameras Nikon D50 and Canon EOS 500D, gives an increased optical radiation intensity areas location representation (both in the region of plasma contraction to the dielectric ledge, and separate strong channels on the upper wall).

The thermal radiation from the dielectric surface inside the discharge section panoramic visualization was carried out through transparent side windows using a Telops FAST M200 infrared (IR) camera (thermal imager) with a spectral range of 1.5 – 5.1 μm. The thermal imaging recording (F) frequency and the one frame exposure (t_e) varied depending on the recorded area specified dimensions and were: F = 500 – 1500 fps and t_e = 0.2 – 1.0 ms, respectively.

3. Thermal radiation non-stationary fields visualization during the pulsed surface discharges initiation in a quiescent gas.

In order to analyze the time of discharge thermal effect on the channel walls surface, the thermal fields dynamics of the dielectric surfaces heated as a result of the discharge plasma initiation was studied and compared with the optical glow time (and the time of the shock-wave effect on the medium) at various initial pressure values.

When a discharge is initiated in quiescent air on the lower wall, the results of discharge plasma optical glow frame-by-frame recording show that in the first 50–100 ns the lower plasma sheet optical radiation is almost uniform, except for the directly obstacle region 6 mm long. The discharge current duration was recorded from current oscillograms and was about 300–500 ns in the case of the discharge initiation at an initial pressure of P ~ 90–125 Torr. By this time, the frame-by-frame images show the effect of surface discharge displacement towards the dielectric insert – an increase in the lower plasma sheet glow intensity in the dielectric insert area. After the discharge current (after 300 ns) end, this enhanced plasma glow relaxes over a time of about 0.7 – 1.5 microseconds [11]. Optical radiation from the upper plasma sheet initiated on the upper flat wall remains uniform (a set of parallel plasma microchannels 30 mm long is uniformly distributed over the surface of a 100 mm long dielectric) and quickly relaxes after the discharge current is completed.

A significant part of the infrared radiation thermal fields generated inside the chamber due to plasma and shock-wave processes is transmitted by quartz windows. If there is such a partially transparent medium between the object under study and the IR camera object-glass, all reflections and total absorption of this medium must also be taken into account. In this case, the registered radiation varies depending on the wavelength, the windows surface state, and their temperature. The object emissivity value can also change depending on the angle at which the emitting object is seen. These limitations do not allow reliable quantitative measurements of the absolute temperature in the heated region. However, thermographic visualization makes it possible to study the spatial and temporal thermal field characteristics and analyze the heat transfer mechanism in the corresponding regions.

To correctly convert the detected radiation into radiation temperature values, it is necessary to determine the following parameters: the object emissivity, the surrounding objects ef-

fective temperature, the atmosphere temperature, and the distance between the thermal imager and the object (to calculate the atmosphere transmission) [12, 13].

With the help of IR imaging in the discharge chamber, it was recorded that the induced discharge plasma noticeably heats the channel wall surface in the test region. The increased visible range glow areas are sources of more intense local heating. When a plasma sheet is initiated in quiescent air on the discharge section upper wall, the main heat exchange mechanism providing wall heating is thermal conductivity (heating of the wall by the plasma). Then, in the absence of plasma, wall cooling is observed through the heat conduction mechanisms.

When a surface discharge is initiated on the channel lower wall, wall surface and ledge pulsed heating occurs locally. Due to contact with the plasma sheet, the channel walls temperature and the ledge temperature increase both by heat exchange with the high-intensity plasma (ledge side surfaces) and due to heating by the flow behind the moving shock wave from the discharge. The experimental data analysis and thermographic images processing were carried out using the Reveal IR program. The color palette was selected on the program toolbar. The dimensionless intensity on the thermograms is given in conventional units.

Figure 2 (a) – (c) shows thermal imaging images obtained with frame-by-frame thermal radiation visualization (F = 1000 fps, t_e = 0.6 ms) from the lower channel wall dielectric surfaces in the insertion region. The surface discharge was initiated in quiescent air with 124 ± 2 Torr initial pressure. Frames (a) – (c) show the thermographic imaging results after applying a filter and subtracting the background to eliminate disproportionate brightness. At the same time, the intensity according to the data obtained from the first frame (Fig. 2 (a)) initially significantly exceeded the intensity recorded in subsequent thermal imaging frames.

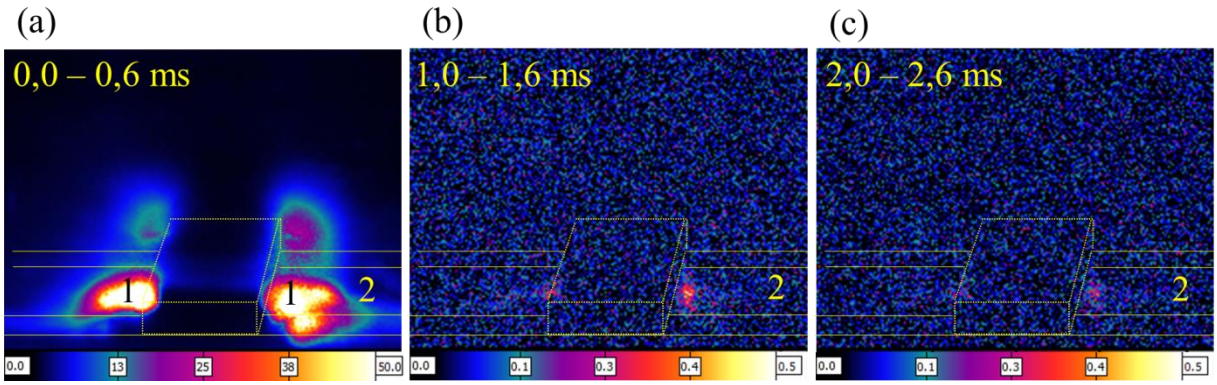

Figure 2. 1 –heating area, 2 – plasma sheet (the interelectrode registered area).

The data analysis in a wide range of air pressures and shooting conditions has shown that, as a result of the surface discharge plasma self-localization, the ledge region remains heated much longer than the channel flat upper wall heated by a sufficiently uniform surface discharge. Due to the significant difference in the characteristic times of the processes occurring during the nanosecond surface discharge initiation, the first IR frame often includes the discharge plasma and subsequent thermal radiation from the heated region (channel walls) recorded during the exposure time. The thermogramms of the recorded heat fluxes from the walls were processed with averaging over the increased intensity region. It was shown that the walls post-discharge cooling time in the plasma displacement zones near a rectangular dielectric profile can reach 20 ms; the flat wall cooling time is up to 3 – 4 ms. The first frame in the images' series, which includes the plasma glow interval, is not shown in the plot of thermal radiation versus time for various initial pressures (presented on Fig. 3). The shooting frequency of the lower wall is F = 629 fps, the upper one is F = 1417 fps.

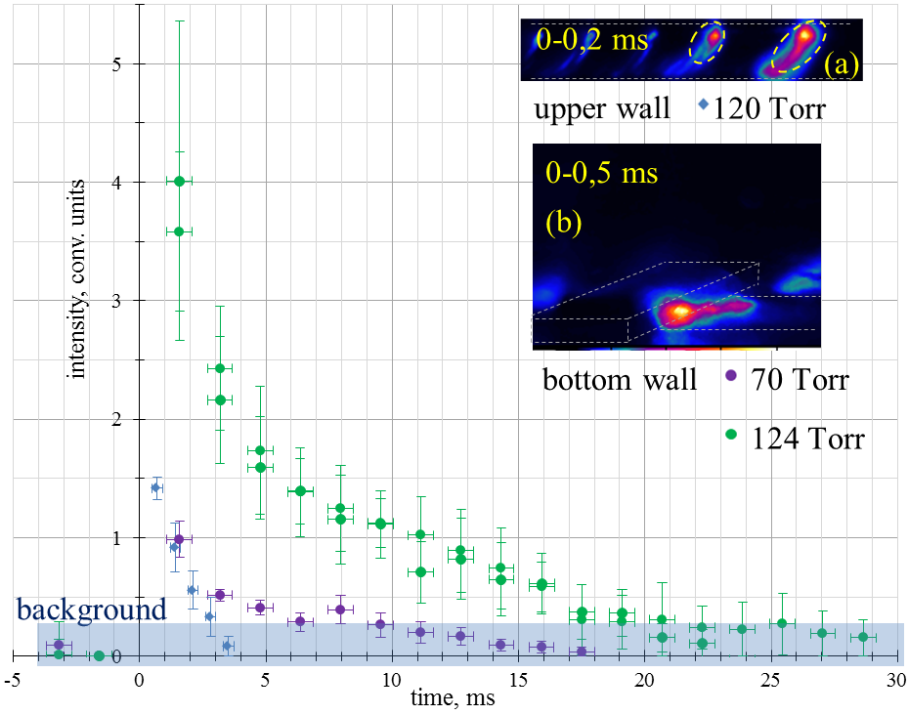

Figure 3. Locally heated regions cooling: (a) the channel upper wall regions (120 Torr), (b) the lower wall area near the dielectric insert (70 Torr, 124 Torr), intensity – in relative units.

4. Thermal radiation non-stationary fields visualization during the pulsed surface discharges initiation in a flow.

Thermal imaging was used to visualize thermal fields formed after the diffraction of a falling plane shock wave (SW) with a Mach number of M_{SW} = 2.8 – 3.2 on a rectangular ledge (forward and backward steps). The gas temperature change at the shock wave front and in the supersonic flow behind it leads to a corresponding change in the heat fluxes time on the streamlined surfaces, in particular, in the flow stagnation zone in front of the obstacle.

After the shock wave had passed over the dielectric ledge front step, a pulsed surface discharge was initiated in the flow behind it in the discharge section channel with various delays t_p. Upon pulsed discharge initiation in the lower section wall region with a ledge, the discharge plasma is distributed in the low-density zones in the form of short-lived high-current plasma channels. IR radiation from regions heated by a short-lived plasma formation was recorded by a thermal imager. To analyze the thermal effect duration, the locally heated by the discharge plasma regions cooling times were studied and compared with the data obtained during the channel sections cooling in the flow without initiating the discharge, which were subsequently used to form the background.

The delay time between the flat shock wave passages windward obstacle wall moment and the pulsed surface discharge initiation moment varied within t_p = 0.1 – 0.4 ms. At this temporal interval, the flow velocity is quite high: 800–700 m/s [9]. The delay time choice makes it possible to initiate the discharge at different flow development stages. With the passage of time, the co-flow behind the leaved shock wave velocity decreases, and the flow becomes turbulent. The discharge repartition occurs in accordance with the change in the flow pattern when the flow passes around a dielectric obstacle.

At short delays after the shock wave passage of the obstacle leading edge, channel walls surfaces are surrounded by a supersonic flow. Figure 4 (a) shows a high-speed shadow frame in 0.06 ms after the shock wave has passed the obstacle front edge. As a shock wave diffraction result, a vortex is formed on the backward step (a reduced density zone behind the step, see corresponding density field numerical simulation in Fig. 4 (b)). The vortex moves downstream. The surface discharge initiated in this flow regime is visualized as a short-lived plas-

ma formation localized in the vortex zone, which is a transverse plasma channel 30 mm long, parallel to the obstacle side wall (Fig. 4 (c) – (f)). The discharge plasma integral glow frames in the visible range are shown in Figs. 4 (d), (f), t_p = 0.06 and 0.34 ms, respectively. As a result, there is a channel wall section adjacent to the plasma region short-term heating (Fig. 4 (c), (e): the thermal field IR frames after the discharge plasma initiation, frame exposure t_e = 1.0 ms).

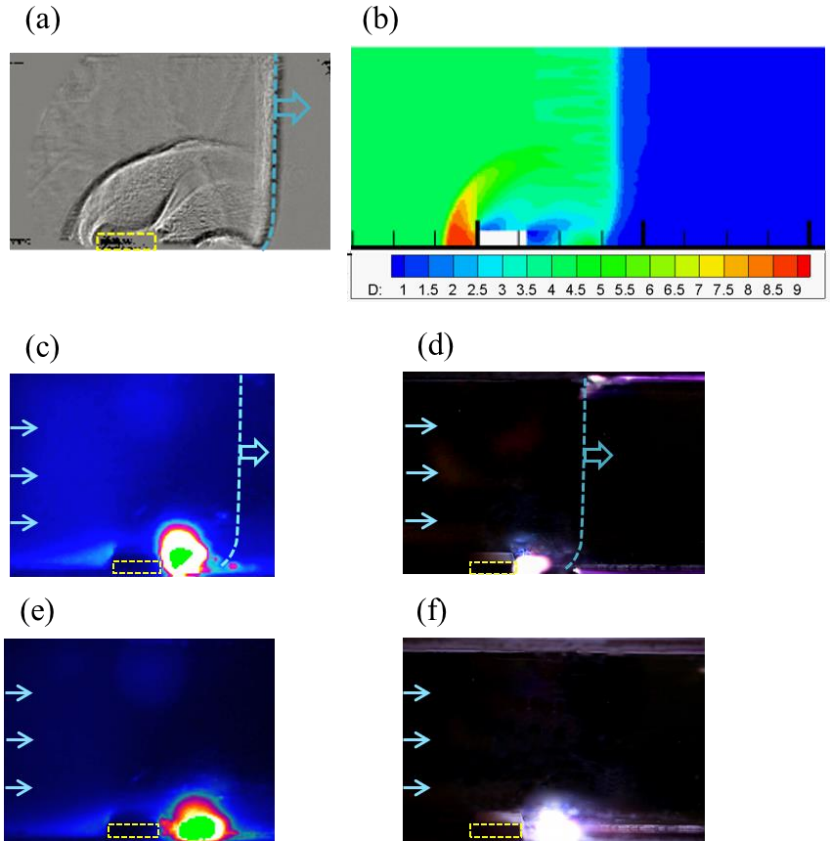

Figure 4. The thermal fields visualization: (a) shadow frame visualizing the flow area behind the reverse step in a supersonic flow behind a flat shock wave; (b) the density field numerical calculation; (c), (e) thermal imaging frames; (d), (f) integral glow images.

The thermal effect from the surface discharge initiation is significant only in the first hundreds microseconds after the discharge plasma initiation – the pulsed heated region quickly moves downstream, the heat dissipates.

In 1 – 2 ms after the discharge plasma relaxation, the thermal radiation intensity from the channel walls in the downwind region, locally heated by the plasma channel, coincides with the background within the error.

Figure 5 shows serial flow region images following discharge initiation in the flow after a flat shock wave (M_{SW} = 3.0 ± 0.2): t_p = 0.34 ms after the shock wave passed. Frequency 1000 fps, frame exposure 0.6 ms, shooting angle 5°. The actual heated stagnation region intensity decreases with time, from frame (a) to frame (d). Frames (b) – (d) demonstrate the channel section thermal field intensity relaxation in the stagnation zone. When visualizing in Figure 5 (a), another filter was applied to reduce the difference in the discharge emission intensity and the stagnation zone.

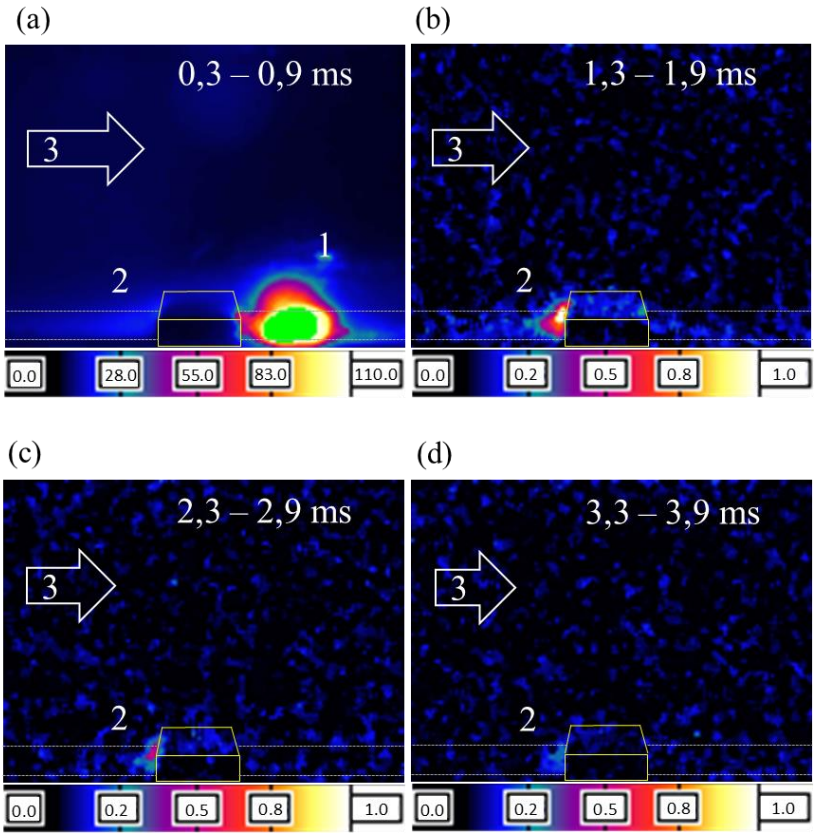

Figure 5. Thermal imaging frames: (1) – discharge localized in the vortex region, (2) – flow stagnation region, (3) – flow direction.

Thermal radiation after the discharge initiation in the flow behind a plane shock wave thermographic recording (t_p = 0.2 – 0.4 ms) was carried out from different angles. The first frame of high-speed shooting in the IR range and the integrated optical image visual comparison gives an idea of the areas locally heated by the discharge plasma and the areas that reflect heat fluxes but are not in contact with the discharge plasma location. Figure 6 shows the results of discharge plasma radiation visualization in the IR (Fig. 6 (a)) and in the visible range (Fig. 6 (b)), initiated in the flow behind a flat shock wave (M_{SW} = 3.8) after 0.2 ms after the shock wave has passed the obstacle forward edge. When shooting heat flows at an angle (Fig. 6 (a) – the angle between the normal to the side walls surface and the thermal imager lens is about 35°), on the first thermographic frame there are various artifacts that arise due to the radiation reflection from copper electrodes, which have a higher coefficient reflections than dielectric surfaces, and the discharge chamber side quartz walls reflections. Similar artifacts are also observed in the discharge plasma optical radiation integrated images. The thermal imaging frequency was 589 fps, exposure 1.0 ms. With such exposure parameters, the areas that emit or reflect heat fluxes for a long time (up to 1 ms) are most clearly recorded on the thermogram. At the same time, in the optical glow integral images obtained with a nanosecond exposure (300–500 ns), in addition to the main regions (1 – 4 in Fig. 6), there are also regions of intense radiation, such as individual nanosecond discharge microchannels and their reflections. However, during thermographic recording, IR radiation from the respective areas is averaged over a longer time. In this case, individual nanosecond heat fluxes (and their reflections) may have a significantly lower (averaged over the microsecond exposure time) intensity compared to the radiation from the main discharge plasma localization region or not be distinguished at all, approaching the background intensity values.

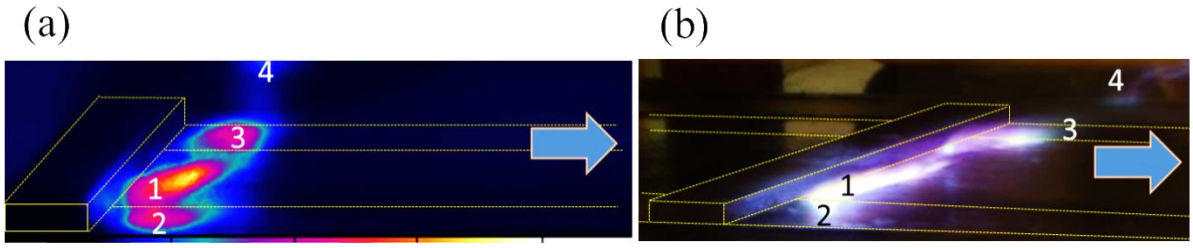

Figure 6. Visualization of (a) recorded radiation in the IR range and (b) surface discharge plasma optical glow integral image: 1 – discharge localized in the vortex region, 2, 3 – discharge radiation reflected by the electrode surface, 4 – radiation reflection on the side wall.

5. Conclusion.

Based on infrared thermography with high temporal and spatial resolution in the 1.5 – 5.1 μm range, panoramic visualization of thermal fields was carried out. An experimental study of non-stationary processes during profiled rectangular channel sections heating and cooling after pulsed surface discharges was carried out, taking into account the supersonic flows structure.

Heating and cooling spatio-temporal characteristics of channel walls with an obstacle after a high-current surface discharge initiation were studied 1) in the quiescent gas, 2) in a high-speed flow behind a plane shock wave with a Mach number of 2.8 – 3.8.

It was shown that the maximum time of thermal radiation from the area heated by the discharge can extent to 20 ms at quischent air. The radiation relaxation times of the thermal fields from dielectric channel walls, locally heated by the discharge, recorded by the thermal imager, lasted for 1 – 2 ms in a high-speed flow behind the shock wave when the surface discharge was localized in the downwind region (at electrical impulse time delays up to 0.4 ms after the shock wave passage).

Acknowledgements

This work was supported by the Russian Science Foundation grant 22-29-00652.

References

[1] Rodrigues F., Pascoa J., Trancossi M. Heat generation mechanisms of DBD plasma actuators // Experimental Thermal and Fluid Science, Vol 90, 2018, pp. 55–65.

[2] Jukes T. N., Choi K.-S., Johnson G. A, Scott S. J. Characterization of surface plasmainduced wall flows through velocity and temperature measurements // AIAA Journal, Vol. 44, № 4, 2006, pp. 764–771.

[3] Starikovskt A. Yu., Alexandrov N. L. Gasdynamic flow control by superfast local heating in a strongly nonequilibrium pulse plasma // Fizika Plazmy, Vol. 47, № 2, 2021, pp. 126–192. [in Russian]

[4] Zhou S., Su L., Shi T., Zheng T., Tong Y., Nie W., Che X., Zhao J. Experimental study on the diffusive flame stabilization mechanism of plasma injector driven by AC dielectric barrier discharge // Journal of Physics D: Applied Physics, Vol. 52, № 26, 2019, 265202.

[5] Zheng H., Liang H., Chen J., Zong H., Meng X., Xie L., Li Y. Experimental study on plasma actuation characteristics of nanosecond pulsed dielectric barrier discharge // Plasma Science and Technology, Vol. 24, № 1, 2022, 015505.

[6] Chen J., Liang H., Wu Y., Wei B., Zhao G., Tian M., Xie L. Experimental Study on Anti-Icing Performance of NS-DBD Plasma Actuator // Applied Sciences, Vol. 8, № 10, 2018, pp. 1889.

[7] Liu Y., Kolbakir C., Hu H., Starikovskiy A., Miles R.B. An experimental study on the thermal characteristics of NS-DBD plasma actuation and application for aircraft icing mitigation // Plasma Science and Technology, Vol. 28, № 1, 2019, 014001.

[8] Ombrello T., Blunck D.L., Resor M. Quantified infrared imaging of ignition and combustion in a supersonic flow // Experiments in Fluids, Vol. 57, № 9, 2016, pp. 1–12.

[9] Znamenskaya I.A., Koroteeva E.Y., Timokhin M.Y., Mursenkova I.V., Glazyrin F.N., Tatarenkova D.I. Experimental investigation of the flow dynamics and boundary layer in a shock tube with discharge section based on digital panoramic methods // International Conference on the Methods of Aerophysical Research (ICMAR 2018): AIP Conference Proceedings, Vol. 2027, 2018, 030161 (doi: 10.1063/1.5065255).

[10] Tatarenkova D. I., Koroteeva E. Y., Kuli-zade T. A., Karnozova E. A., Znamenskaya I. A., Sysoev N. N. Pulsed discharge-induced high-speed flow near a dielectric ledge // Experiments in Fluids, Vol. 62, № 7, 2021, 151 (doi: 10.1007/s00348-021-03253-0).

[11] Extrusion of a nanosecond surface discharge plasma near a dielectric ledge / I. Znamenskaya, D. Tatarenkova, I. Mursenkova, T. Kuli-Zade, E. Karnozova // Journal of Physics: Conference Series, Vol. 2100, 2021, 012010 (doi:10.1088/1742-6596/2100/1/012010).

[12] Astarita T., Carlomagno G.M. Infrared Thermography For Thermo-Fluid-Dynamics. Springer Science & Business Media, 2012, 226 p.

[13] Znamenskaya I.A. Methods for Panoramic Visualization and Digital Analysis of Thermophysical Flow Fields. A Review // Scientific Visualization 13.3, 2021, pp. 125 – 158, (doi: 10.26583/sv.13.3.13).